Transmission-Line Bandpass Filter Structures With Infinite Reflectionless Range

Jongheun Lee, *Graduate Student Member, IEEE*, and Juseop Lee, *Senior Member, IEEE*

***Abstract*— This article is to present a complete method to design transmission-line reflectionless filters. Our approach can be used to accord a transmission-line filter to feature an infinite frequency range of reflectionless response. It can be applied to reflectionless filter prototypes consisting of filtering and matching sections that comply the Cauer topology. Hence, it does not limit by the filter order and/or the filter response type. Design equations supporting our approach are provided, and their applications to actual filter designs will be elaborated via various filter examples with distinct features. The measurements authenticate our design approach.**

***Index Terms*— Absorptive filters, reflectionless filters.**

I. Introduction

In recent, filters with constant input impedance, dubbed as reflectionless filters, have been introduced. The core theory is to make a filter have a frequency-invariant input impedance matched to the port impedance. Synthesis techniques capitalize on the even- and odd-analysis of a symmetric two-port network [1]–[4], the concept of balanced circuitries [5], or complement matching sections [6]–[15]. This work focuses on the third one which has the largest number of applications compared to the others.

As briefly mentioned in the previous paragraph, one of the ideas to build a reflectionless filter is to add a matching section to a port, intended to dissipate the reflection. It originates from the multiplexer theory, where each channel filter is synthesized and designed under assuming that the voltage source has zero inherent resistance (*i.e.* singly terminated filters). Accordingly, the element values of the filtering section are the ones of singly terminated filters [16], and the matching section is configured such that the input impedance constantly amounts to the port impedance.

By virtue of its simplicity, a number of filter designs using distributed elements are available in documents. The work in [9] sought methods to reduce the number of resonators in use. Design methods of frequency-tunable reflectionless filters can be found in [10]. It is possible to build a bilateral reflectionless filter by simultaneously adding a matching section to each port [11]. Recent interests involve seeking methods to broaden the reflectionless range of actual reflectionless filters.

In theory, an ideal reflectionless filter is expected to produce zero reflection at all frequencies. In practice, however, a good return loss can be observed within a limited frequency range, *e.g.* $0.5f_0$–$1.5f_0$ (f_0: center frequency), as reported by articles [8]–[12], which are the pioneering works on transmission-line reflectionless filters. This discord between theory and practice is caused by ignoring the frequency-variant (dispersive) feature of actual transmission-line inverter. Although there have been handful of attempts to increase the impedance-matching range of a transmission-line reflectionless bandpass filter, only a few works have focused on this issue. A large proportion of recent approaches empirically draft a transmission-line schematic for a reflectionless bandpass filter, followed by seeking the design parameters that minimize the reflection through long-winded design equations or numerical optimization techniques, which are believed to be impractical.

This article presents a classic but powerful method to design a transmission-line filter featuring an infinite frequency range of reflectionless response. Our method facilitates synthesizing a coupled-line schematic from a reflectionless filter prototype, and it has its basis on rigorous circuit transformations. Hence, the derivation of a practical filter schematic can be carried out without depending on experimental attempts. Explicit design equations are given in terms of the filter specifications, so that a bandpass filter can be systematically designed subsequent to the synthesis of a lowpass prototype circuit.

II. Inverter-Coupled Lowpass Prototype

Our method can be used to make a transmission-line bandpass filter have an infinite reflectionless range when its lowpass prototype has the filtering and matching sections conforming to Cauer topologies. Our first discussion proceeds with the one capable of producing the Butterworth transmission response with zero reflections at all frequencies, and its circuit diagram is shown in Fig. 1(a). The g-parameters of its filtering section are the ones of singly terminated Butterworth filters [16], and those of the matching section are the reciprocals of each g-parameter in the filtering section ($g_{f,i} = 1/g_{m,i}$).

In general, designing resonator filters begins with building an inverter-coupled circuit by placing inverters between every pairs of elements (ports, inductors, and capacitors). This work suggests not to position an inverter at the starting point of the filtering section, since its dispersiveness would have a direct

Manuscript received 26 November 2021; revised 4 February 2022; accepted 1 March 2022. Date of publication 16 March 2022; date of current version 27 May 2022. This work was supported by the National Research Foundation of Korea (NRF) through the Korean Government [Ministry of Science and ICT (MSIT)] under Grant 2022R1A2B5B01001340. This article was recommended by Associate Editor K. Moez. *(Corresponding author: Juseop Lee.)*

The authors are with the Department of Radio Communications Engineering, Korea University, Seoul 02841, South Korea (e-mail: juseoplee@gmail.com).

Digital Object Identifier 10.1109/TCSI.2022.3157323

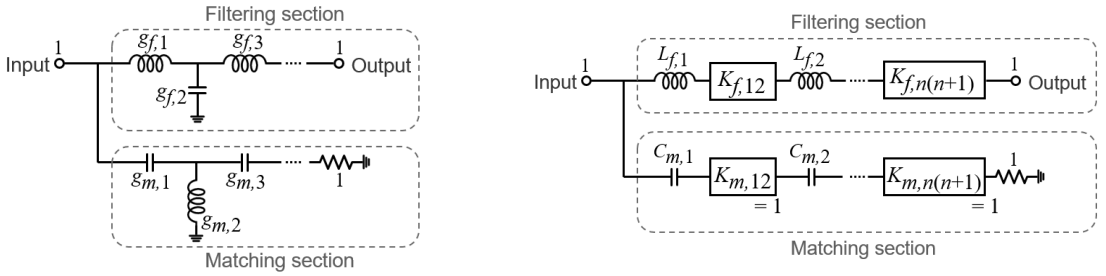

(a) (b)

Fig. 1. nth-order Butterworth reflectionless filter. (a) Lowpass prototype circuit. (b) Inverter-coupled circuit equivalent to (a).

impact on the filtering section's input admittance. Specifically, it severely increases the degree of the frequency-variant feature of the input admittance, making it seriously deviated from the desired stopband input admittance, acquired under the premise that the inverters are ideal. Separately, whether or not having a frequency-variant inverter as the first element of the matching section makes little difference in the overall input admittance of the filter under certain conditions, which will be discussed soon after. The proposed inverter-coupled circuit is shown in Fig. 1(b).

The transformation formulae can be derived by equating the input admittance of each section in Fig. 1(b) with that of the corresponding one in Fig. 1(a), which gives

$$K_{f,i(i+1)} = \sqrt{\frac{L_{f,i} \cdot L_{f,i+1}}{g_{f,i} \cdot g_{f,i+1}}}$$
$$K_{f,n(n+1)} = \sqrt{\frac{L_{f,n}}{g_{f,n}}}, \tag{1}$$

where $L_{f,1} = g_{f,1}$, as the first element of the filtering section has no degree of freedom. The element values in the matching section can also be derived in the same manner, and they can be expressed as

$$K_{m,i(i+1)} = \sqrt{\frac{g_{m,i} \cdot g_{m,i+1}}{C_{m,i} \cdot C_{m,i+1}}}$$
$$K_{m,n(n+1)} = \sqrt{\frac{g_{m,n}}{C_{m,n}}}, \tag{2}$$

where $C_{m,1} = g_{m,1}$.

In theory, an inverter-coupled filter has an infinite number of inverter value sets for a specific frequency response. However, the impedances of the matching-section inverters do affect the stopband matching performance when they are dispersive. This can be attributed to the fact that the input admittance seen at the input port becomes more subject to the matching section's input admittance as the frequency deviates from the passband frequencies. Based on the fact that a frequency-variant inverter line terminated by a resistor has a frequency-invariant constant input impedance when the line impedance is the same with the resistance, this work recommends to set each matching-section capacitor value such that all the matching-section inverters are unit inverters:

$$C_{m,i} = g_{m,i} \tag{3}$$

TABLE I
ELEMENT VALUES OF SECOND-ORDER BUTTERWORTH REFLECTIONLESS FILTERS

Fig. 1(a)	$g_{f,1}$	$g_{f,2}$		$g_{m,1}$	$g_{m,2}$
	1.4142	0.7071		0.7071	1.4142
Fig. 1(b)	$^1L_{f,1}$	$K_{f,12}$	$K_{f,23}$	$C_{m,1}$	$C_{m,2}$
	1.4142	1.4142	1.4142	0.7071	1.4142

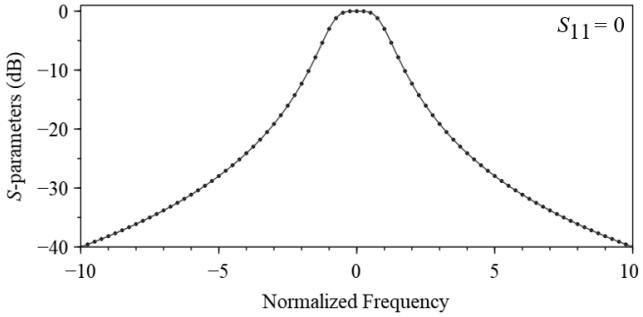

Fig. 2. Response of the second-order Butterworth reflectionless lowpass filter. Circles: response of Fig. 1(a) with the values in Table I. Solid line: response of Fig. 1(b) with the values in Table I. Plots for S-parameters are the same.

Separately, the filtering-section inverters have a small impact on the actual return loss performance that can be neglected.

Fig. 2 shows the frequency responses of the circuits in Fig. 1. In this demonstration, the element values are the ones which produce the second-order Butterworth response, and the values for Fig. 1(b) were found by using equations (1)-(3) under the condition that $g_{f,i} = g_{f,1}$ for all i.

To sum up, this chapter discussed two critical design rules:

1) An inverter must not be used as the first element of the filtering section.
2) The impedances of the matching-section inverters should be set to unity.

It is worth highlighting that this work investigates the sources that limit impedance-matching range of an actual reflectionless filter, and proposes the analysis-based design rules.

III. TRANSMISSION-LINE BANDPASS CIRCUIT WITH STUBS

The next step is to apply the lowpass-to-bandpass transformation, the impedance scaling, and the *Richard's*

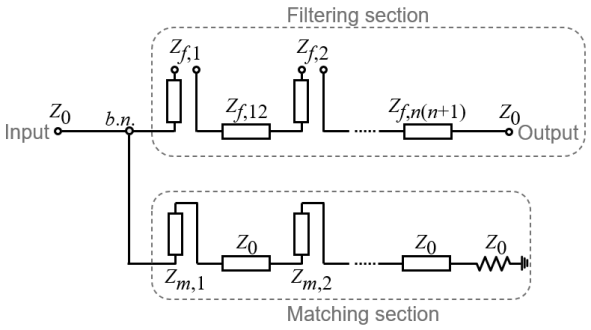

Fig. 3. nth-order reflectionless bandpass filter with line inverters and stubs.

transformation to the normalized inverter-coupled lowpass circuit in Fig. 1(b) so as to obtain the stub-based bandpass circuit shown in Fig. 3.

Lowpass-to-Bandpass Transformation: This transforms the inductors and the capacitors into series and parallel resonators, respectively. Its details are not shown in this article as they are incorporated in the following equations describing the impedances of the stubs.

Impedance Scaling: The impedance scaling applied to the ports and the matching-section resistor leads to the port and the matching-resistor impedance of Z_0. The impedance scaling of the rest of the elements are incorporated in the following equations describing the line impedances.

Richard's Transformation: A $\lambda_0/4$ (λ_0: wavelength at the center frequency) open-circuited series stub is equivalent to a series-*LC* resonator connected in series [17]. Its impedance can be found from the value of the inductor from which the series resonator originates, as given by

$$Z_{f,i} = \frac{4Z_0 L_{f,i}}{\pi \Delta}, \tag{4}$$

where Z_0 and are the denormalized port impedance and the target fractional bandwidth. Similarly, a capacitor in series can be transformed into a short-circuited series stub with having the impedance of [17]

$$Z_{m,i} = \frac{\pi Z_0 \Delta}{4C_{m,i}}. \tag{5}$$

Each impedance inverter in the inverter-coupled lowpass circuit corresponds to a $\lambda_0/4$ transmission line in the distributed-element circuit. The characteristic impedance is given by

$$Z = Z_0 \cdot K, \tag{6}$$

where K is the impedance of each inverter in Fig. 1(b).

Fig. 4 shows the transmission and reflection responses of the circuit in Fig. 3 with the impedances in the first row of Table II and the theoretical response of the second-order Butterworth reflectionless bandpass filter having the fractional bandwidth of 0.05. As all lines are quarter-wavelength long at the center frequency, the response between DC-$2f_0$ repeats every $2f_0$. It can be observed that the proposed circuit in Fig. 3 produces the transmission response (solid line) that is indistinguishable from the prespecified Butterworth transmission response (Circles), validating our design concept. Despite of the fact that the stub circuit contains frequency-variant line inverters, it has the return loss larger than 30 dB over the entire frequency range, which cannot typically be obtained from optimization-based transmission-line structures.

TABLE II

IMPEDANCES (Ω) OF SECOND-ORDER BUTTERWORTH REFLECTIONLESS FILTER WITH DIFFERENT Δ ($Z_0 = 50\ \Omega$)

Δ	[1]$Z_{f,1}$	$Z_{f,12}$	$Z_{f,23}$	$Z_{m,1}$	$Z_{m,2}$
0.05	1800.62	70.71	70.71	2.777	1.388
0.10	900.31	70.71	70.71	5.554	2.776
0.15	600.21	70.71	70.71	8.331	4.164
0.20	450.16	70.71	70.71	11.108	5.552

[1] $Z_{f,1} = Z_{f,2}$.

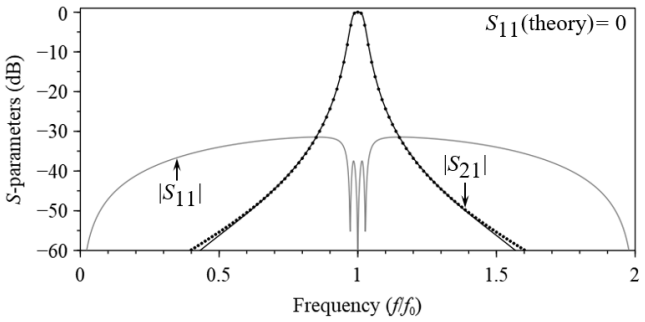

Fig. 4. Frequency responses of the second-order Butterworth reflectionless bandpass filters of $\Delta = 0.05$. Circles: theory. Solid lines: simulated response of the schematic in Fig. 3 with the line impedances of Table II.

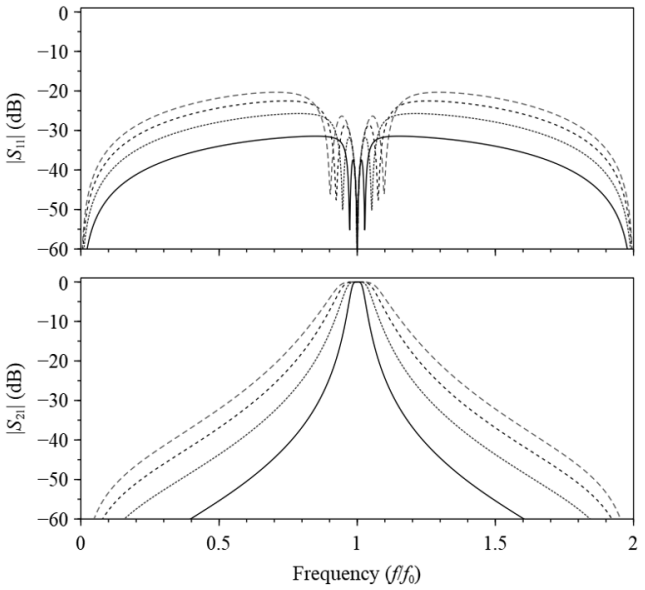

Fig. 5. Transmission and reflection responses of the schematic in Fig. 3 with the parameters in Table II. $\Delta = 0.05$ (solid lines), 0.1 (dotted lines), 0.15 (short-dashed lines), and 0.2 (long-dashed lines).

A. Bandwidth

As can be seen in equations (4) and (5), the filter bandwidth can be controlled by having a different Δ when computing

TABLE III
IMPEDANCES (Ω) OF HIGHER-ORDER BUTTERWORTH FILTERS ($Z_0 = 50\ \Omega$ AND $\Delta = 0.05$)

n	$^1Z_{f,1}$	$Z_{f,12}$	$Z_{f,23}$	$Z_{f,34}$	$Z_{f,45}$	$Z_{f,56}$	$Z_{m,1}$	$Z_{m,2}$	$Z_{m,3}$	$Z_{m,4}$	$Z_{m,5}$
3	1909.86	53.03	91.86	86.60			2.945	2.618	0.982		
4	1948.95	49.36	58.58	118.9	100.0		3.006	3.097	2.125	0.751	
5	1967.28	47.75	50.49	69.49	147.0	111.8	3.034	3.327	2.714	1.756	0.607

$^1Z_{f,1} = Z_{f,i}$ for i = 2, 3, ..., n.

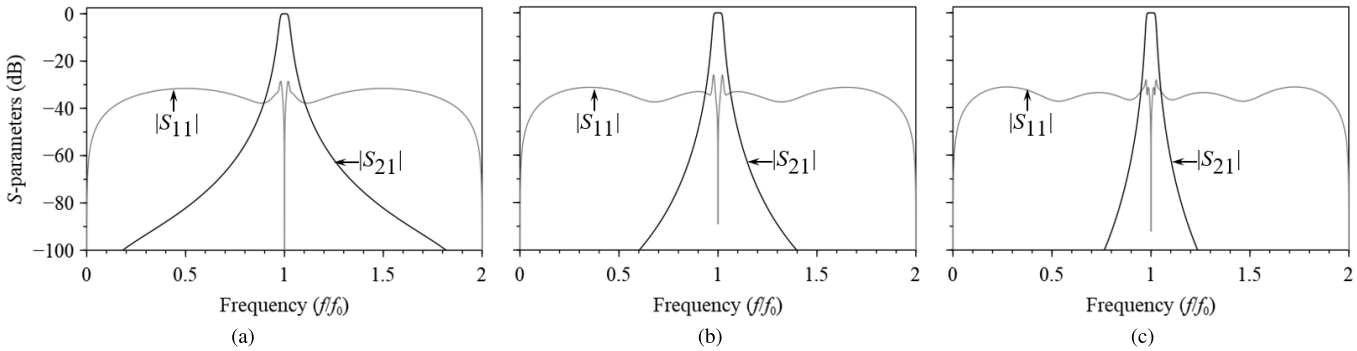

Fig. 6. Transmissions and reflections of the schematic in Fig. 3 with the impedances in Table III. (a) $n = 3$. (b) $n = 4$. (c) $n = 5$.

each stub impedance as shown in Table II. Note that the impedances of the line inverters do not change by Δ, as they only vary by the g-parameters in use. The power transmission and reflection responses of each example are plotted in Fig. 5. Even though the return loss varies with the bandwidth due to the frequency-variant features of the line inverters, the frequency responses indicate that high-performance reflectionless bandpass filters with a moderate bandwidth can be realized in practice.

B. Higher-Order Filters

Our approach is not limited by the filter order. For example, Table III lists the line impedances of the circuit in Fig. 3 for producing the Butterworth transmission responses of orders 3, 4, and 5. Their power transmission and reflection responses are plotted in Fig. 6. All three examples produce $|S_{11}|$ smaller than −30 dB over the entire frequency range, indicating that

- The proposed design rules guarantee an infinite frequency range of reflectionless response regardless of the order of the filter.
- The filter order does not have a significant impact on the minimum return loss.

Note that all filter structures produce zero reflection when all of their inverters are frequency-invariant.

IV. COUPLED-LINE BANDPASS CIRCUIT

The feasibility of the schematic in Fig. 3 depends on finding an equivalent coupled-line circuit, as it contains series stubs that are challenging to be implemented in practice. Given that the schematic is built by two subcircuits connected in parallel at the bifurcation node, this work suggests to individually find a coupled-line structure that is equivalent to each section.

A. Filtering Section

The values of the filtering-section inverters can be chosen at will, as they do not critically affect the overall return loss performance of the filter when implemented with dispersive line inverters. This implies that an infinite number of solution sets exist, allowing us to arbitrarily determine all the inductor values except for $L_{f,1}$ in Fig. 1(b), beforehand. In this article, we impose the condition that all inductors except for the nth-inductor in Fig. 1(b) have the inductance of

$$L_{f,i} = g_{f,1}, \tag{7}$$

for $i = 1, 2, \ldots, n$-1. Equation (7) determines all the filtering-section inverter values except for the last two as

$$K_{f,i(i+1)} = \frac{g_1}{g_i \cdot g_{i+1}}. \tag{8}$$

for $i = 1, 2, \ldots n$-2.

The diagram of the transmission-line circuit is redrawn in Fig. 7(a). All stub impedances except for the nth stub are set to $Z_{f,1}$. The impedances of the line inverters except for the last two can be found by using equations (6) and (8). A $\lambda_0/4$ line of impedance Z_0 has been inserted between the input port and the bifurcation node, and it does not alter the magnitude of the filter response. The stubs except for the nth stub are equally split into two such that each has the impedance of $Z_{f,1}/2$. The stub of impedance $Z_{f,n}$ has been unequally split into two of impedances $Z_{f,1}/2$ and ($Z_{f,n}$ - $Z_{f,1}/2$).

Matched-Transformer-Ratio Condition: Transforming the first and the (n+1)th sections into coupled lines delivers two transformers of ratios 1:r and s:1, respectively. At this point, r and s must be the same as to have the port impedance unaltered from Z_0. To this end, the following condition must

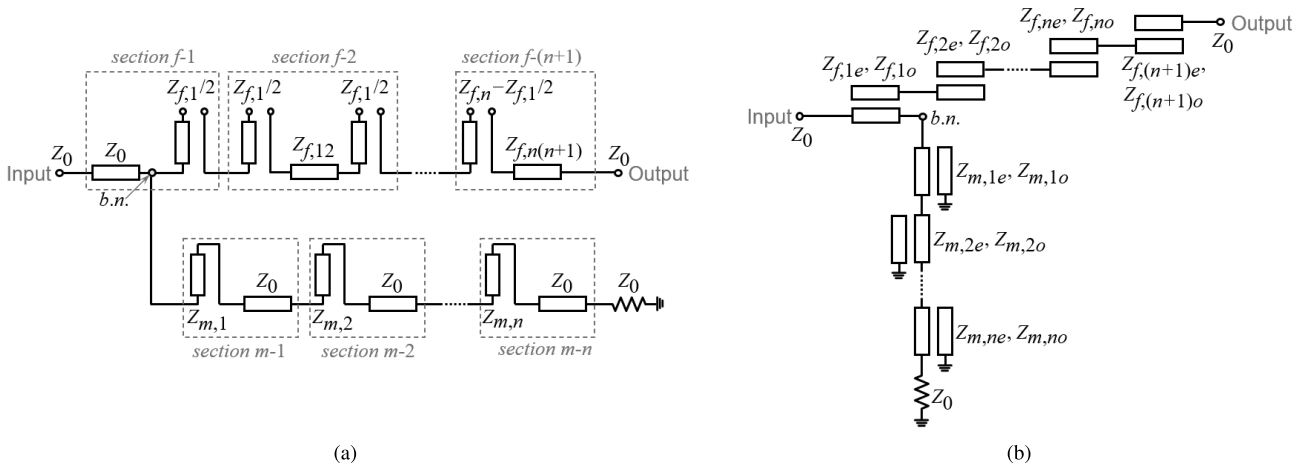

Fig. 7. nth-order Butterworth input-reflectionless bandpass filter. (a) Circuit schematic with line inverters and stubs. (b) Circuit schematic with coupled lines.

be satisfied:

$$\frac{Z_{f,1}}{2Z_0} = \frac{2Z_{f,n} - Z_{f,1}}{2Z_{f,n(n+1)}}, \tag{9}$$

which mandates the nth-inductor value in Fig. 1(b) to be

$$L_{f,n} = \frac{g_{f,1}}{8} \cdot (4 + k \pm \sqrt{k^2 + 8k}), \tag{10}$$

where

$$k = \frac{g_{f,1}}{g_{f,n}}.$$

Observe that $L_{f,n}$ solely depends on the g-parameters in use. Plugging it into equation (1) gives the last two inverter values as

$$K_{f,(n\text{-}1)n} = \sqrt{\frac{g_{f,1}}{g_{f,n\text{-}1}}} \cdot \sqrt{\frac{k}{8} \cdot (4 + k \pm \sqrt{k^2 + 8k})}$$
$$K_{f,n(n+1)} = \sqrt{\frac{k}{8} \cdot (4 + k \pm \sqrt{k^2 + 8k})} \tag{11}$$

The undetermined line impedances of Fig. 7(a) can be found by using equations (4) and (6) with (10) and (11).

Provided that equations (7)-(11) are satisfied, the filtering section in Fig. 7(a) can be implemented with coupled lines as shown in Fig. 7(b). It has the modal impedances of

$$Z_{f,1e} = Z_0 \cdot (1 + 1/r)$$
$$Z_{f,1o} = Z_0 \cdot (1 - 1/r)$$
$$Z_{f,(n+1)e} = Z_{f,n(n+1)} \cdot (1 + 1/r)$$
$$Z_{f,(n+1)o} = Z_{f,n(n+1)} \cdot (1 - 1/r), \tag{12}$$

for the first and the $(n+1)$th sections, and

$$Z_{f,ie} = \frac{4Z_{f,i(i+1)} + Z_{f,1}}{2r^2}$$
$$Z_{f,io} = \frac{Z_{f,1}}{2r^2}, \tag{13}$$

for the intermediate sections, where

$$r\ (= s) = \sqrt{1 + \frac{Z_{f,1}}{2Z_0}}, \tag{14}$$

according to equation (9).

B. Matching Section

As all the design parameters of the matching section have been determined in equations (2), (3), (5), and (6), it can be transformed into the coupled-line structure shown in Fig. 7(b). Each short-circuited series stub and the following inverter line [sections m-i in Fig. 7(a)] can be paired up and transformed into a pair of coupled lines with the modal impedances of

$$Z_{m,ie} = Z_{m,i} + Z_0 + \sqrt{Z_{m,i} \cdot (Z_{m,i} + Z_0)}$$
$$Z_{m,ie} = Z_{m,i} + Z_0 - \sqrt{Z_{m,i} \cdot (Z_{m,i} + Z_0)}, \tag{15}$$

for $i = 1, 2, \ldots, n$.

V. Verification

In order to elaborate the design process discussed so far, a filter example having a second-order Butterworth response has been designed, fabricated, and measured. Our design guideline can be outlined in the five steps below:

1) Select a filter response and synthesize its g-parameters.
2) Set each $C_{m,i}$ of the inverter-coupled circuit in Fig. 1(b) to the corresponding g-parameter ($g_{m,i}$), and find $K_{m,i(i+1)}$ (indeed they are unity).
3) Let each $L_{f,i}$ ($i \neq n$) be $g_{f,1}$, and determine $L_{f,n}$ in step with the matched-transformer-condition. Then, find each $K_{f,i(i+1)}$ using the determined inductor values.
4) Convert the inductors, capacitors, and inverters to stubs and lines. The target fractional bandwidth (Δ) should be specified in this step and applied to these equations.
5) Transform the stub circuit to an equivalent coupled-line circuit.

The step-by-step procedure with actual values are given below.

Step I: The lowpass prototype of an nth-order Butterworth input-reflectionless filter is shown in Fig. 1(a). It produces the second-order Butterworth response when

$$g_{f,1} = 1.4142$$
$$g_{f,2} = 0.7071, \tag{16}$$

and

$$g_{m,1} = (g_{f,1})^{-1} = 0.7071$$
$$g_{m,2} = (g_{f,2})^{-1} = 1.4142. \quad (17)$$

as indicated in Table I.

Step II: We then set each matching-section capacitor value to its corresponding g-parameter as

$$C_{m,1} = g_{m,1} = 0.7071$$
$$C_{m,2} = g_{m,2} = 1.4142. \quad (18)$$

Plugging the capacitor values into equation (2) gives

$$K_{m,12} = K_{m,23} = 1.0. \quad (19)$$

as indicated in Fig. 1(b).

Step III: The inductor values can be found from equations (7) and (10) as

$$L_{f,1} = 1.4142$$
$$L_{f,2} = 0.27 \text{ or } 1.8512. \quad (20)$$

Equation (10) that finds $L_{f,2}$ (=$L_{f,n}$) has two possible solutions, and the larger value of $L_{f,2}$ has been chosen in this exercise. The inverter values can be found from equation (11) as

$$K_{f,12} = K_{f,23} = 1.618. \quad (21)$$

It is required to further make use of equation (8) when finding the inverter values of a filter with $n > 2$.

Step IV: The target center frequency and bandwidth are set to 2 GHz and 0.1 GHz ($\Delta = 0.05$), respectively. The diagram of the stub circuit is depicted in Figs. 3 and 7(a). Its impedances can be found by plugging the lowpass-domain parameters in (18)-(21) into equations (4)-(6), which gives

$$Z_{f,1} = 1800.62\ \Omega$$
$$Z_{f,2} = 2357.04\ \Omega$$
$$Z_{f,12} = Z_{f,23} = 80.9\ \Omega. \quad (22)$$

and

$$Z_{m,1} = 2.777\ \Omega$$
$$Z_{m,2} = 1.388\ \Omega, \quad (23)$$

under the condition that $Z_0 = 50\ \Omega$.

Step V: The modal impedances of the coupled-line circuit in Fig. 7(b) can be obtained from equations (12)-(15) with the line impedances in (22) and (23) as

$$r = s = 4.3596$$
$$Z_{f,1e} = 61.49\ \Omega$$
$$Z_{f,1o} = 35.83\ \Omega$$
$$Z_{f,2e} = 55.88\ \Omega$$
$$Z_{f,2o} = 47.37\ \Omega$$
$$Z_{f,3e} = 99.46\ \Omega$$
$$Z_{f,3o} = 62.34\ \Omega. \quad (24)$$

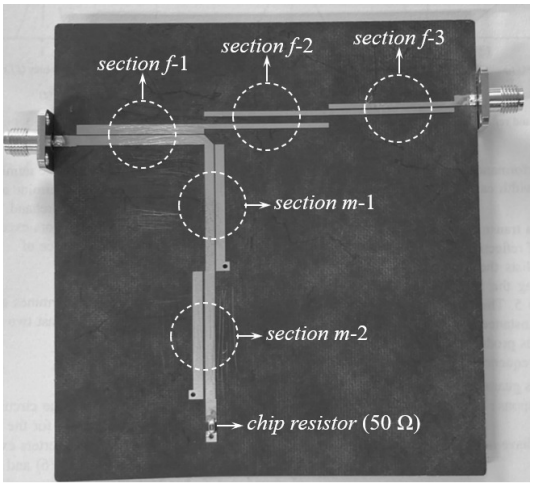

Fig. 8. Top-view of the fabricated second-order Butterworth filter. $w_{f,1} = 2.17$, $s_{f,1} = 0.19$, $l_{f,1} = 27.7$, $w_{f,2} = 1.08$, $s_{f,2} = 1.70$, $l_{f,2} = 27.7$, $w_{f,3} = 1.04$, $s_{f,3} = 0.38$, $l_{f,3} = 28.0$, $w_{m,1} = 2.04$, $s_{m,1} = 0.24$, $l_{m,1} = 28.0$, $w_{m,2} = 2.19$, $s_{m,2} = 0.47$, and $l_{m,2} = 27.8$. w, s, and l stand for the width, spacing, and length of the coupled lines of each section. All dimensions are in mm.

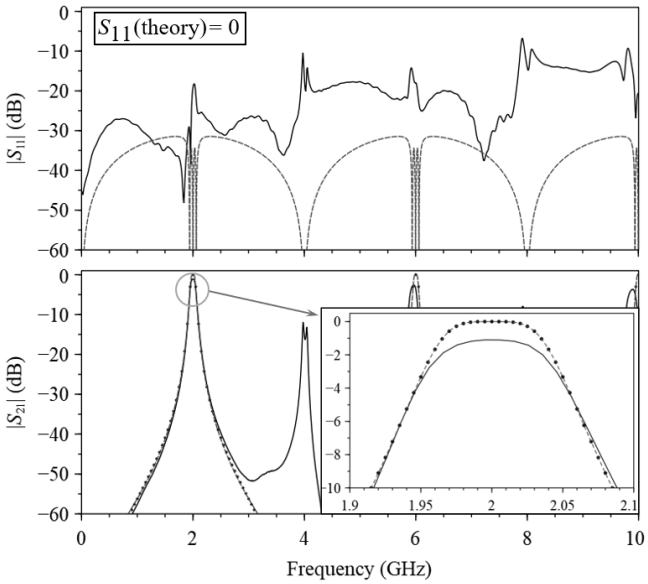

Fig. 9. Measured responses (solid lines) of the fabricated filter in Fig. 8, the circuit simulation result (dashed lines) of the coupled-line circuit in Fig. 7(b), and the theoretical response (circles) of the second-order Butterworth reflectionless bandpass filter.

and

$$Z_{m,1e} = 64.88\ \Omega$$
$$Z_{m,1o} = 40.67\ \Omega$$
$$Z_{m,2e} = 59.84\ \Omega$$
$$Z_{m,1o} = 42.94\ \Omega. \quad (25)$$

To verify the design method and the parameters discussed in this chapter, we have fabricated and measured the designed coupled-line filter. It has been implemented by microstrip lines on a 0.787mm-thick-Rogers 5880 substrate ($\varepsilon_r = 2.2$), of which the dimensions were found by typing in the modal

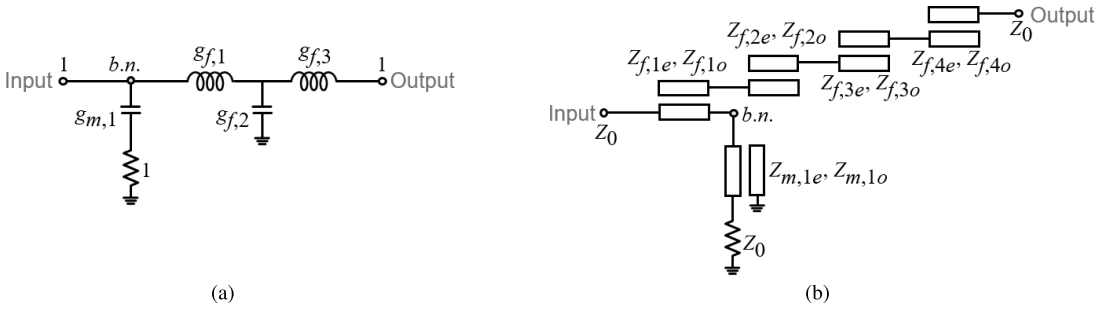

Fig. 10. Semi-reflectionless filter. (a) Lowpass prototype circuit. (b) Coupled-line bandpass filter.

TABLE IV
DESIGN PARAMETERS OF THE CIRCUITS IN FIG. 10

Fig. 10(a)	$g_{f,1}$	$g_{f,2}$	$g_{f,3}$		$g_{m,1}$
	1.5472	1.0870	0.6591		1.1193
[1]Fig. 10(b)	$Z_{f,1e}$	$Z_{f,2e}$	$Z_{f,3e}$	$Z_{f,4e}$	$Z_{m,1e}$
	65.18	56.39	65.39	118.6	67.21
	$Z_{f,1o}$	$Z_{f,2o}$	$Z_{f,3o}$	$Z_{f,4o}$	$Z_{m,1o}$
	34.82	45.39	45.39	63.35	39.81

[1]The impedances (Ω) are for a response with $\Delta = 0.1$ and $Z_0 = 50$ Ω.

impedances in (24) and (25) into AWR line calculator tool. The top-view of the fabricated microstrip-line circuit is shown in Fig. 8.

Fig. 9 shows the circuit simulated responses of the coupled-line circuit schematic in Fig. 7(b) with the modal impedances in (24) and (25), and the measured responses of the fabricated filter in Fig. 8. The predefined Butterworth response is plotted as well for comparison. Observe that all $|S_{21}|$ agree with one another at frequencies in and close to the passband, confirming the validity of our approach. The fabricated filter has the return loss overall larger than 10 dB within the range from DC to 8 GHz ($=4f_0$). The unwanted peaks near 4 GHz and 8 GHz are due to the unequal modal phase velocities of coupled lines in an inhomogeneous medium (*e.g.* microstrip environment). The maximum $|S_{11}|$ at the passband frequencies is measured to be -17.8 dB, which is satisfactory in consideration of fabrication errors. The sensitivity analyses on filter dimensions inform that the matching performance at these frequencies highly depends on the errors in section f-1 rather than the others.

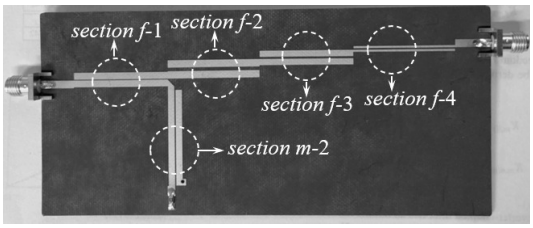

Fig. 11. Top-view of the fabricated semi-reflectionless bandpass filter. $w_{f,1} = 2.10$, $s_{f,1} = 0.15$, $l_{f,1} = 27.7$, $w_{f,2} = 2.26$, $s_{f,2} = 0.96$, $l_{f,2} = 27.1$, $w_{f,3} = 1.93$, $s_{f,3} = 0.50$, $l_{f,3} = 27.4$, $w_{f,4} = 0.72$, $s_{f,4} = 0.33$, $l_{f,4} = 28.5$, $w_{m,1} = 1.96$, $s_{m,1} = 0.25$, and $l_{m,1} = 28.0$. All dimensions are in mm.

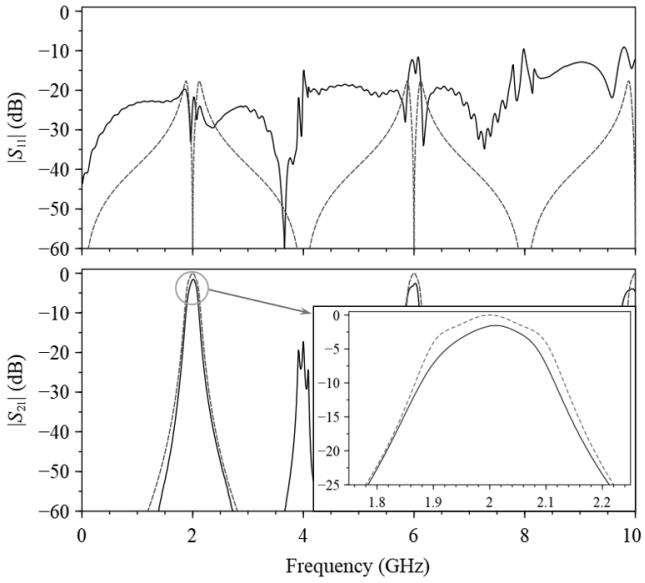

Fig. 12. Measured responses (solid lines) of the fabricated filter in Fig. 11 and the simulation results (dashed lines) of the schematic in Fig. 10(b).

VI. APPLICATION

This chapter demonstrates the versatility and universality of our design method using five different filter examples.

A. Smaller Number of Elements in the Matching Section

An nth-order reflectionless filter featuring a canonical transmission response along with a perfect impedance matching has no fewer than $2n$ resonators. The work in [9] proposed a semi-reflectionless lowpass prototype that contains fewer resonators in the matching section.

1) Lowpass Prototype: For example, the lowpass prototype in Fig. 10(a) has one susceptive element in its matching section. Its parameters can be found by meas of the synthesis technique in [9], and those for a response with a return loss larger than 18 dB at all frequencies are summarized in Table IV.

2) Coupled-Line Circuit: The coupled-line circuit schematic is depicted in Fig. 10(b). The impedances in Table IV are for a bandpass response centered at 2 GHz with

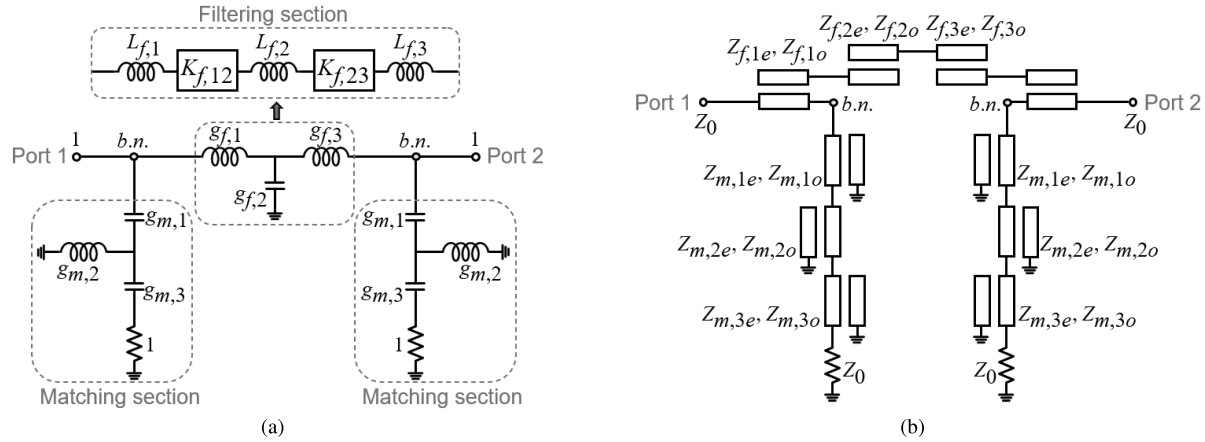

Fig. 13. Bilateral semi-reflectionless filter. (a) Lowpass prototype circuit. (b) Coupled-line bandpass filter.

TABLE V
DESIGN PARAMETERS OF THE CIRCUITS IN FIG. 13

Fig. 13(a)	[1]$g_{f,1}$	$g_{f,2}$	$g_{m,1}$	$g_{m,2}$	$g_{m,3}$
	1.3584	1.9559	0.6748	0.5418	0.8694
[4]Fig. 13(b)	[2]$Z_{f,1e}$	[3]$Z_{f,2e}$	$Z_{m,1e}$	$Z_{m,2e}$	$Z_{m,3e}$
	66.10	53.45	73.86	77.62	70.21
	[2]$Z_{f,1o}$	[3]$Z_{f,2o}$	$Z_{m,1o}$	$Z_{m,2o}$	$Z_{m,3o}$
	33.90	44.82	37.80	36.88	38.82

[1]$g_{f,1} = g_{f,3}$ due to symmetry.
[2]$Z_{f,1(e,o)} = Z_{f,4(e,o)}$ due to symmetry.
[3]$Z_{f,2(e,o)} = Z_{f,3(e,o)}$ due to symmetry.
[4]The impedances (Ω) are for a response with $\Delta = 0.1$ and $Z_0 = 50$ Ω.

the 3-dB bandwidth of 200 MHz ($\Delta = 0.1$). It has been fabricated using microstrip lines, and its photograph is shown in Fig. 11. The lines were etched on top of the same Rogers substrate used in the previous example. Fig. 12 shows the simulation results of the coupled-line circuit in Fig. 10(b) with the impedances in Table IV, and the measurements of the fabricated microstrip-line filter. The measured return loss is larger than 10 dB up to 10 GHz ($=5f_0$) as expected.

B. Reflectionless Response at Both Ports

1) Lowpass Prototype: A bilateral reflectionless filter can be made by using two matching sections as depicted in Fig. 13(a). Its g-parameters can be found by means of the optimization techniques in [11], and a response the minimum return loss of 15 dB can be achieved with the values listed in Table V.

2) Inverter-Coupled Lowpass Prototype: Port 2 in Fig. 13(a) has a matching section as is the case with port 1. Hence, it is suggested not to place an inverter between the inductor, $g_{f,3}$, and the bifurcation node at port 2, since it becomes a critical inverter that deteriorates $|S_{22}|$ when it is dispersive. The dashed box between the ports in Fig. 13(a) shows the inverter-coupled of the filtering section. As it is symmetric ($g_{f,1} = g_{f,3}$), we do not have to be concerned about the matching-transformer-ratio condition. Hence, it is preferred to set

$$L_{f,\mathrm{i}} = g_{f,1}, \tag{26}$$

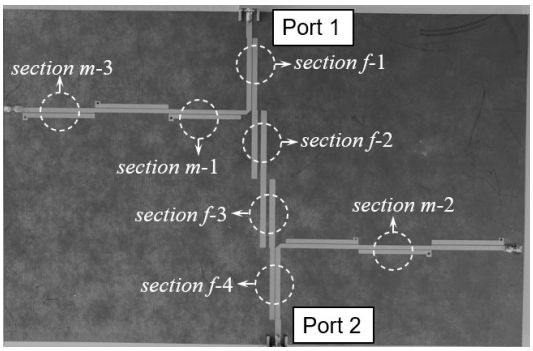

Fig. 14. Top-view of the fabricated bilateral semi-reflectionless filter. $w_{f,1} = w_{f,4} = 2.06$, $s_{f,1} = s_{f,4} = 0.13$, $l_{f,1} = l_{f,4} = 27.9$, $w_{f,2} = w_{f,3} = 2.40$, $s_{f,2} = s_{f,3} = 1.20$, $l_{f,2} = l_{f,3} = 27.0$, $w_{m,1} = 1.75$, $s_{m,1} = 0.15$, $l_{m,1} = 28.4$, $w_{m,2} = 1.65$, $s_{m,2} = 0.12$, $l_{m,2} = 28.5$, $w_{m,3} = 1.86$, $s_{m,3} = 0.22$, and $l_{m,3} = 28.3$. All dimensions are in mm.

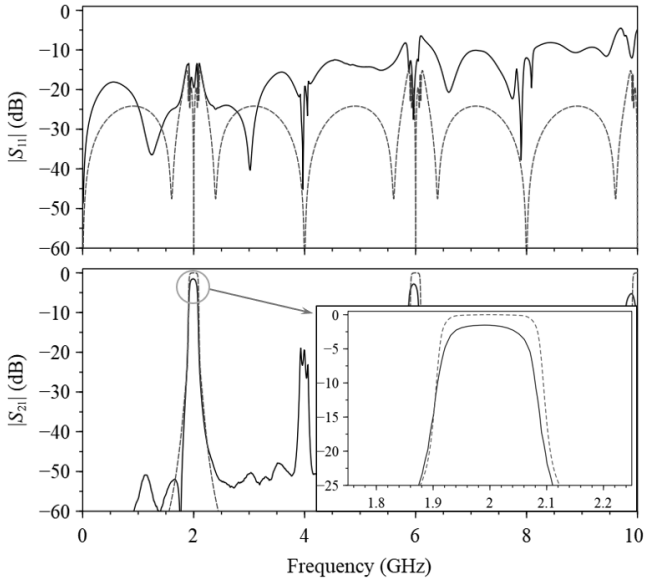

Fig. 15. Measured responses (solid lines) of the fabricated filter in Fig. 14 and the simulation results (dashed lines) of the schematic in Fig. 13(b).

for $i = 1, 2, \ldots, n$. The filtering-section inverter values can be found by plugging $L_{f,i}$ in (26) into equation (1). The schematic of the matching section is the same with the one shown in

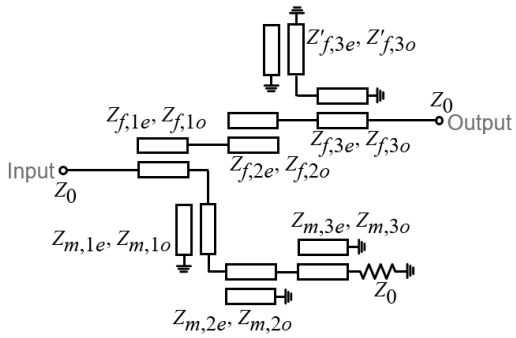

Fig. 16. Third-order inverse-Chebyshev input-reflectionless filter made with coupled lines (stopband ripple: −14.43 dB).

TABLE VI

IMPEDANCES (Ω) OF THIRD-ORDER INVERSE-CHEBYSHEV BANDPASS FILTER (STOPBAND RIPPLE: −14.43 DB, $Z_0 = 50\ \Omega$, AND $\Delta = 0.05$)

$Z_{f,1e}$	$Z_{f,2e}$	$Z_{f,3e}$	$Z'_{f,3e}$	$Z_{m,1e}$	$Z_{m,2e}$	$Z_{m,3e}$
60.31	60.31	70.26	58.03	63.15	63.15	58.75
$Z_{f,1o}$	$Z_{f,2o}$	$Z_{f,3o}$	$Z'_{f,3o}$	$Z_{m,1o}$	$Z_{m,2o}$	$Z_{m,3o}$
39.69	39.69	38.81	51.05	41.38	41.38	43.52

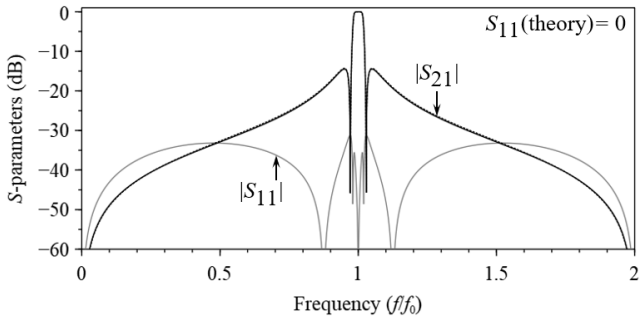

Fig. 17. Frequency response of the third-order inverse-Chebyshev bandpass filter. Dotted lines: theoretical response. Solid lines: simulated response of the schematic in Fig. 16 with the impedances in Table VI. The dotted and solid lines for $|S_{21}|$ are indistinguishable.

Fig. 1(b), and its capacitor values can be found by plugging each $g_{m,\mathrm{i}}$ in Table V into equation (3).

3) Coupled-Line Circuit: Finding the design parameters of the coupled-line schematic in Fig. 13(b) can be executed by using equations (4)-(6) with the calculated lowpass parameters, followed by utilizing equations (12)-(15). $Z_{f,n(n+1)}$ in equation (12) must be replaced to Z_0 as the inverter-coupled circuit in Fig. 13(a) does not contain $K_{f,n(n+1)}$. The impedances in Table V are the ones for a bandpass response of $\Delta = 0.1$.

The fabricated filter and its measured response are shown in Figs. 13 and 14, respectively. $|S_{22}|$ of the circuits are not shown as they are equal or similar to their counterparts.

C. Inverse-Chebyshev Response

1) Lowpass Prototype: An inverse-Chebyhsev response has transmission zeros at real frequencies. Its synthesis method for input-reflectionless filters was presented in [7], and its lowpass prototype can be formulated by modifying the even-numbered filtering-section capacitors in Fig. 1(a) to shunt Foster sections. The prototype diagram can be found in [7].

2) Coupled-Line Circuit: Finding a feasible schematic for an inverse-Chebyshev filter requires to deal with transmission-line Foster sections. The detailed design method of these structures are given in [18]. Note that the matching section is identical to those of Butterworth filters of the same order. The impedances in Table VI are for a bandpass response of $\Delta = 0.05$.

The simulation results of the schematic in Fig. 16 are shown in Fig. 17. The theoretical response of the inverse-Chebyshev filter is plotted as well for comparison. In can be observed that an input-reflectionless filter with transmission zeros prescribed by the canonical characteristic function can be made to have an infinite reflectionless range when implemented with distributed elements, which highlights the universality of our approach.

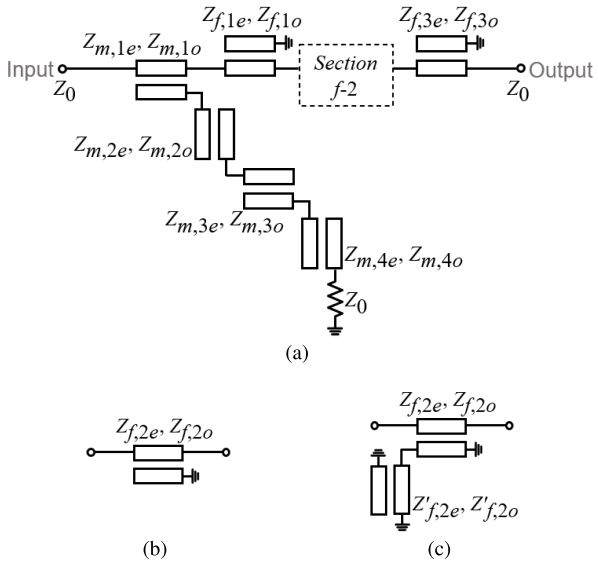

Fig. 18. (a) Coupled-line schematic of a third-order bandstop filter. (b) *Section f*-2 of a Butterworth filter. (c) *Section f*-2 of an inverse-Chebyshev filter.

TABLE VII

IMPEDANCES (Ω) OF THIRD-ORDER BUTTERWORTH BANDSTOP FILTER ($Z_0 = 50\ \Omega$ AND $\Delta = 0.05$)

$Z_{f,1e}$	$Z_{f,2e}$	$Z_{f,3e}$	$Z_{m,1e}$	$Z_{m,2e}$	$Z_{m,3e}$	$Z_{m,4e}$
65.43	64.36	58.06	61.15	52.79	59.05	133.69
$Z_{f,1o}$	$Z_{f,2o}$	$Z_{f,3o}$	$Z_{m,1o}$	$Z_{m,2o}$	$Z_{m,3o}$	$Z_{m,4o}$
40.46	40.88	43.91	38.85	47.51	47.51	84.93

TABLE VIII

IMPEDANCES (Ω) OF THIRD-ORDER INVESE-CHEBYSHEV BANDSTOP FILTER (STOPBAND RIPPLE: −20 DB, $Z_0 = 50\ \Omega$, AND $\Delta = 0.05$)

$Z_{f,1e}$	$Z_{f,2e}$	$Z'_{f,2e}$	$Z_{f,3e}$	$Z_{m,1e}$	$Z_{m,2e}$	$Z_{m,3e}$	$Z_{m,4e}$
68.93	72.12	57.84	55.66	63.63	50.03	52.98	113.76
$Z_{f,1o}$	$Z_{f,2o}$	$Z'_{f,2o}$	$Z_{f,3o}$	$Z_{m,1o}$	$Z_{m,2o}$	$Z_{m,3o}$	$Z_{m,4o}$
39.23	38.27	38.81	45.39	36.37	42.54	39.59	65.03

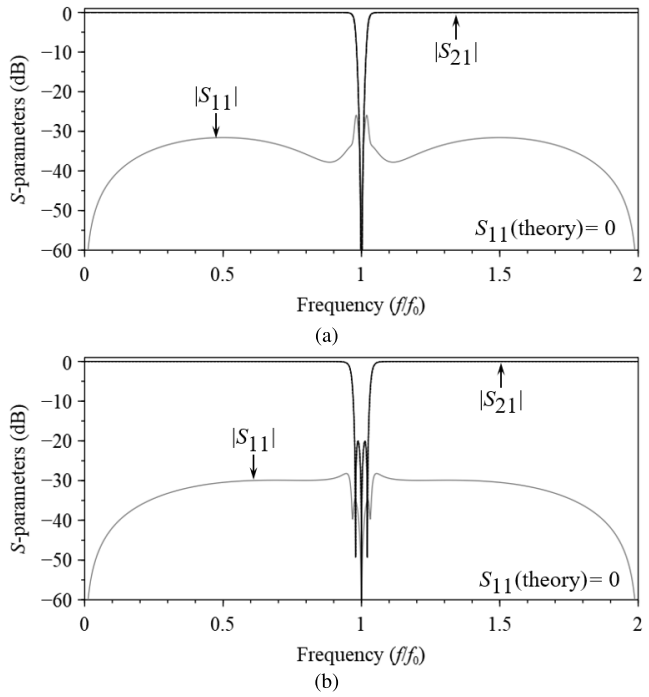

Fig. 19. Frequency responses of the coupled-line bandstop filters. Dotted lines: theoretical response. Solid lines: simulated response. (a) Butterworth response. (b) Inverse-Chebyshev response. The dotted and solid lines for $|S_{21}|$ are indistinguishable.

D. Bandstop Response

The schematic of a bandstop filter can be found by applying the lowpass-to-bandstop transformation to the inverter-coupled lowpass circuit in Fig. 1(b). This transforms each inductor into a parallel-*LC* pair, and each capacitor into a series-*LC* pair. The inverter values depend on the choice of each lumped-element value, and for bandstop filters, it is suggested to set as

$$L_{f,i} = g_{f,i}. \tag{27}$$

The Richard-equivalent stubs of the *LC* pairs were discussed in Chapter III. The impedance of the short-circuited series stub in the filtering section can be written in terms of the inductor value from which it originates:

$$Z_{f,i} = \frac{\pi Z_0 \Delta L_{f,i}}{4}. \tag{28}$$

The matching section contains open-circuited series stubs with the impedance of

$$Z_{m,i} = \frac{4Z_0}{\pi \Delta C_{m,i}}. \tag{29}$$

In brief, the stub schematic of a bandstop filter can be made by exchanging the output port and matching resistor in Fig. 3,

1) Coupled-Line Circuit: The process of finding the coupled-line schematic of a bandstop filter is highly similar to the one discussed in Chapter IV. Rather than repeating the process in terms of bandstop filters, this section delineates two examples, both of which produce canonical transmission responses.

The coupled-line schematic of a third-order bandstop filter is illustrated in Fig. 18(a). As stated earlier, the even-numbered components in the filtering section of inverse-Chebyshev filters differ from those of Butterworth filters. This results in distinct coupled-line structures in the final circuit schematic as shown in Figs. 18(b) and (c). The line impedances in Tables VII and VIII are for bandstop responses of $\Delta = 0.05$. The *g*-parameters for a 20 dB-inverse-Chebyshev response can be found in [7].

The circuit simulations of the coupled-line bandstop filters are plotted in Fig. 19. The results verify our design approach.

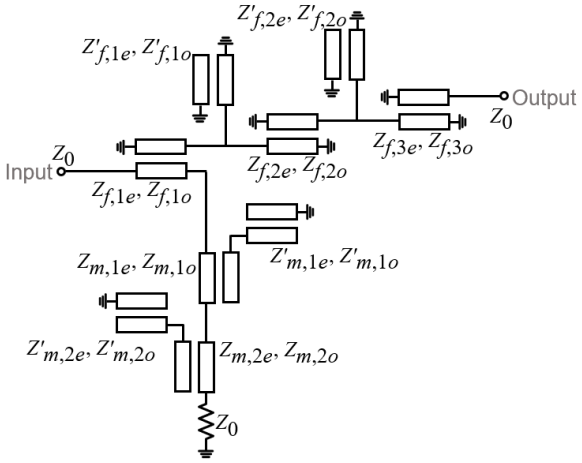

Fig. 20. Coupled-line schematic of a second-order dual-bandpass filter.

TABLE IX
IMPEDANCES (Ω) OF SECOND-ORDER BUTTERWORTH DUAL-BANDPASS FILTER ($Z_0 = 50\ \Omega$)

$Z_{f,1e}$	$Z'_{f,1e}$	$Z_{f,2e}$	$Z'_{f,2e}$	$Z_{f,3e}$	$Z_{m,1e}$	$Z'_{m,1e}$	$Z_{m,2e}$	$Z'_{m,2e}$
69.19	62.69	62.11	53.51	40.67	66.19	55.57	61.76	58.64
$Z_{f,1o}$	$Z'_{f,1o}$	$Z_{f,2o}$	$Z'_{f,2o}$	$Z_{f,3o}$	$Z_{m,1o}$	$Z'_{m,1o}$	$Z_{m,2o}$	$Z'_{m,2o}$
39.14	47.68	48.02	40.67	25.50	33.81	44.76	38.24	47.24

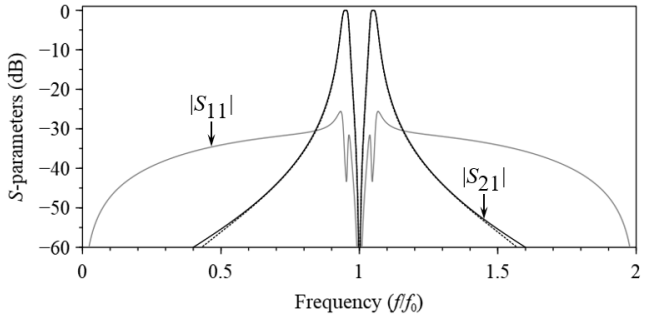

Fig. 21. Frequency response of the coupled-line dual-bandpass filter. Dotted lines: theoretical response. Solid lines: simulated response of the schematic in Fig. 20 with the impedances in Table IX. The dotted and solid lines for $|S_{21}|$ are indistinguishable.

E. Dual-Bandpass Response

A bandpass filter with two passbands can be synthesized by applying the dual-bandpass transformation in [19] to a lowpass prototype. For example, Fig. 20 illustrates the schematic of a

TABLE X
COMPARISON OF THIS WORK WITH RECENT WORKS ON TRANSMISSION-LINE REFLECTIONLESS BANDPASS FILTERS

Ref.	Capable of having a mathematically prescribed $\|S_{21}\|$ (canonical transmission response)	Closed-form synthesis-based equations for given specification (filter response type and bandwidth)	*Maximum $\|S_{11}\|$ at near-passband frequencies ($0.5f_0$–$1.5f_0$)	*Frequency range of reflectionless response ($\|S_{11}\|$ < -10 dB)
[5]	Available	Available	-10 dB (-10 dB)	$0.5f_0$–$1.5f_0$ ($0.5f_0$–$1.5f_0$)
[15]	Available	Available	-15 dB (-22 dB)	DC–$2f_0$ (DC–infinity)
[20]	Not available	Not available	-15 dB (-15 dB)	DC–$1.88f_0$ (DC–infinity)
[21]	Not available	Not available	-10 dB (-15 dB)	$0.25f_0$–$1.5f_0$ ($0.25f_0$–$1.75f_0$)
[22]	Not available	Not available	-10 dB (N/A)	$0.64f_0$–$1.24f_0$ (N/A)
[23]	Not available	Not available	-10 dB (-10 dB)	DC–$2f_0$ (DC–infinity)
[24]	Not available	Not available	-13.5 dB (-19.3 dB)	DC–$2.8f_0$ (DC–infinity)
[25]	Not available	Not available	-8 dB (-10 dB)	$0.66f_0$–$1.44f_0$ ($0.55f_0$–$1.45f_0$)
This work	**Available**	**Available**	**-17.8 dB (-32 dB)**	**DC–$3.8f_0$ (DC–infinity)**

*Figures of merits in parentheses are the ones of ideal circuit simulations.
f_0 of dual-band filters is defined to be the frequency at which the lines are quarter-wavelength ($\lambda_0/4$) long.

dual-bandpass filter, designed such that each passband has a second-order Butterworth response. It was intended that each passband is centered at $0.9f_0$ and $1.1f_0$, respectively, where f_0 is the frequency at which the lines are quarter-wavelength long. Δ were set to 0.025 for both passbands. The design parameters for the specified response are given in Table IX. Its response is plotted in in Fig. 21 along with the prespecified one, and it sufficiently validates the universality of our design approach.

VII. DISCUSSION

The universality and the versatility of our design approach have been verified through six distinct filter examples, each of which features

- a mathematically predefined Butterworth (maximally flat) bandpass response;
- reduced number of elements in the matching section;
- a bilateral reflectionless response;
- a mathematically defined inverse-Chebyshev (maximally flat passband along with transmission zeros at stopband) bandpass response;
- canonical (Butterworth and inverse-Chebyshev) bandstop responses;
- a canonical (Butterworth) dual-bandpass response.

It is worth noting that all six coupled-line filters could have not been designed to produce infinite reflectionless ranges without our two critical design guidelines discussed in Chapter II. Our design process of a high-performance reflectionless filter finds a feasible coupled-line schematic from a given topology, and it is based on rigorous circuit transformations, which absolutely distinguishes our work from others in [20]–[25], which heavily rely on trail-and-error optimizations after empirically drafting a transmission-line filter schematic. Readers may refer to Table X for more quantitative and qualitative comparisons.

VIII. CONCLUSION

This article has presented a universal design approach which enables a distributed-element filter to produce an infinite range of reflectionless response. Feasible coupled-line schematics for reflectionless filters were thoroughly formulated on the basis of circuit transformations, and the design approach was described in terms of a step-by-step procedure so that beginners can fully understand the details. It was guaranteed that transmission-line filters constructed sticking to our design rules produce infinite range of reflectionless response. Closed-form design equations were provided in terms of the lowpass prototype parameters, the center frequency, and the bandwidth so that a coupled-line reflectionless filter can be systematically designed subsequent to a filter synthesis. In accordance, no optimization techniques were required to design our coupled-line filter examples. The versatility of our method was demonstrated through six distinct filter examples. all featuring infinite reflectionless range. Three filters were fabricated, and their measurements exhibited good agreements with the predefined responses. It is anticipated that our method gives impetus to time-efficient methodical designs for reflectionless filters.

REFERENCES

[1] M. A. Morgan and T. A. Boyd, "Reflectionless filter structures," *IEEE Trans. Microw. Theory Techn.*, vol. 63, no. 4, pp. 1263–1271, Apr. 2015.
[2] M. A. Morgan, *Reflectionless Filters*. Norwood, MA, USA: Artech House, 2017.
[3] M. A. Morgan, W. M. Groves, and T. A. Boyd, "Reflectionless filter topologies supporting arbitrary low-pass ladder prototypes," *IEEE Trans. Circuits Syst. I, Reg. Papers*, vol. 66, no. 2, pp. 594–604, Feb. 2019.
[4] J. Lee, B. Lee, S. Nam, and J. Lee, "Rigorous design method for symmetric reflectionless filters with arbitrary prescribed transmission response," *IEEE Trans. Microw. Theory Techn.*, vol. 68, no. 6, pp. 2300–2307, Jun. 2020.
[5] J. Lee and J. Lee, "Generic and versatile reflectionless filter topology and its applications to distributed-element reflectionless bandpass filters," *IEEE Trans. Microw. Theory Techn.*, vol. 69, no. 6, pp. 3058–3069, Jun. 2021.
[6] T.-H. Lee, B. Lee, and J. Lee, "First-order reflectionless lumped-element lowpass filter (LPF) and bandpass filter (BPF) design," in *IEEE MTT-S Int. Microw. Symp. Dig.*, San Francisco, CA, USA, May 2016, pp. 1–4.
[7] M. Khalaj-Amirhosseini and M.-M. Taskhiri, "Twofold reflectionless filters of inverse-Chebyshev response with arbitrary attenuation," *IEEE Trans. Microw. Theory Techn.*, vol. 65, no. 11, pp. 4616–4620, Nov. 2017.
[8] D. Psychogiou and R. Gómez-García, "Reflectionless adaptive RF filters: Bandpass, bandstop, and cascade designs," *IEEE Trans. Microw. Theory Techn.*, vol. 65, no. 11, pp. 4593–4605, Nov. 2017.
[9] S.-W. Jeong, T.-H. Lee, and J. Lee, "Absorptive filter prototype and distributed-element absorptive bandpass filter," in *IEEE MTT-S Int. Microw. Symp. Dig.*, Reykjavik, Iceland, Aug. 2018, pp. 1–4.
[10] S.-W. Jeong, T.-H. Lee, and J. Lee, "Frequency- and bandwidth-tunable absorptive bandpass filter," *IEEE Trans. Microw. Theory Techn.*, vol. 67, no. 6, pp. 2172–2180, Jun. 2019.

[11] R. Gómez-García, J.-M. Muñoz-Ferreras, and D. Psychogiou, "Symmetrical quasi-absorptive RF bandpass filters," *IEEE Trans. Microw. Theory Techn.*, vol. 67, no. 4, pp. 1472–1482, Apr. 2019.
[12] R. Gómez-García, J.-M. Muñoz-Ferreras, and D. Psychogiou, "High-order input-reflectionless bandpass/bandstop filters and multiplexers," *IEEE Trans. Microw. Theory Techn.*, vol. 67, no. 9, pp. 3683–3695, Sep. 2019.
[13] B. Koh and J. Lee, "Reflectionless Butterworth and Chebyshev filters," in *Proc. 1st Eur. Microw. Conf. Central Eur. (EuMCE)*, Prague, Czech Republic, May 2019, pp. 112–115.
[14] S.-W. Jeong and J. Lee, "Absorptive bandpass filter with a pair of transmission zeros," in *Proc. IEEE Int. New Circuits Syst. Conf. (NEWCAS)*, Montreal, QC, Canada, Jun. 2020, pp. 102–105.
[15] J. Lee, J. Lee, and N. S. Barker, "Rigorous design of input-reflectionless filter with Chebyshev response and exact approach to increase reflectionless range," *IEEE Trans. Microw. Theory Techn.*, vol. 69, no. 10, pp. 4460–4475, Oct. 2021.
[16] A. I. Zverev, *Handbook of Filter Synthesis*. Hoboken, NJ, USA: Wiley, 1967.
[17] G. L. Matthaei, L. Young, and E. M. T. Jones, *Microwave Filters, Impedance-Matching Networks, and Coupling Structures*. Dedham, MA, USA: Artech House, 1980.
[18] J. Lee and J. Lee, "Implementation of distributed-element Foster section and its applications to bandpass filters," *IEEE Microw. Wireless Compon. Lett.*, early access, Dec. 23, 2021, doi: 10.1109/LMWC.2021.3135267.
[19] J. Lee and K. Sarabandi, "A synthesis method for dual-passband microwave filters," *IEEE Trans. Microw. Theory Techn.*, vol. 55, no. 6, pp. 1163–1170, Jun. 2007.
[20] X. Wu, Y. Li, and X. Liu, "Quasi-reflectionless microstrip bandpass filters with improved passband flatness and out-of-band rejection," *IEEE Access*, vol. 8, pp. 160500–160514, 2020.
[21] C. Luo *et al.*, "Quasi-reflectionless microstrip bandpass filters using bandstop filter for out-of-band improvement," *IEEE Trans. Circuits Syst. II, Exp. Briefs*, vol. 67, no. 10, pp. 1849–1853, Oct. 2020, doi: 10.1109/TCSII.2019.2946915.
[22] M. Fan, K. Song, L. Yang, and R. Gomez-Garcia, "Frequency-reconfigurable input-reflectionless bandpass filter and filtering power divider with constant absolute bandwidth," *IEEE Trans. Circuits Syst. II, Exp. Briefs*, vol. 68, no. 7, pp. 2424–2428, Jul. 2021.
[23] Y. Zhang, Y. Wu, H. Yu, and W. Wang, "All-frequency absorptive CL dual-band BPF with complementary lossy bandstop branches," *IEEE Trans. Circuits Syst. II, Exp. Briefs*, vol. 68, no. 12, pp. 3532–3536, Dec. 2021.
[24] Y. Zhang, Y. Wu, W. Wang, and J. Yan, "High-performance common-and differential-mode reflectionless balanced band-pass filter using coupled ring resonator," *IEEE Trans. Circuits Syst. II, Exp. Briefs*, early access, Aug. 9, 2021, doi: 10.1109/TCSII.2021.3103535.
[25] Y.-H. Zhu, J. Cai, and J.-X. Chen, "Quasi-reflectionless double-sided parallel-strip line bandpass filter with enhanced selectivity," *IEEE Trans. Circuits Syst. II, Exp. Briefs*, vol. 69, no. 2, pp. 339–343, Feb. 2022.

Jongheun Lee (Graduate Student Member, IEEE) received the B.E. degree in computer and communication engineering from Korea University, Seoul, South Korea, in 2019, where he is currently pursuing the Ph.D. degree in radio communications engineering.

His current research interest includes microwave planar passive circuits.

Juseop Lee (Senior Member, IEEE) received the B.Eng. and M.Eng. degrees in radio science and engineering from Korea University, Seoul, South Korea, in 1997 and 1999, respectively, and the Ph.D. degree in electrical engineering from the University of Michigan, Ann Arbor, MI, USA, in 2009.

He joined the Electronics and Telecommunications Research Institute (ETRI), Daejeon, South Korea, in 2001, where he was involved in the design of passive microwave equipment for Ku- and Ka-band communications satellites. In 2005, he joined the University of Michigan, where he was a Research Assistant and a Graduate Student Instructor at the Radiation Laboratory and was involved in research activities focused on millimeter-wave radars and synthesis techniques for multiple-passband microwave filters. In 2009, he joined Purdue University, West Lafayette, IN, USA, as a Post-Doctoral Research Associate, where he was involved in the design of adaptable RF systems. In 2012, he joined Korea University, where he is currently a Professor. From 2019 to 2020, he was a Visiting Professor at the University of Virginia, Charlottesville, VA, USA. His current research interests include RF and microwave circuits, satellite transponders, and wireless power transfer systems.

Prof. Lee was a recipient of the Best Teaching Award presented by Korea University for Spring 2018 and Fall 2018. He was an Associate Editor of the IEEE TRANSACTIONS ON MICROWAVE THEORY AND TECHNIQUES (2017–2019).